

DETERMINATION OF $\Delta G/G$
IN COMPASS EXPERIMENT AT CERN* **

J.P. NASSALSKI

Andrzej Sołtan Institute for Nuclear Studies
Hoża 69, 00-681 Warsaw, Poland.
e-mail: Jan.Nassalski@fuw.edu.pl*(Received March 18, 1998)*

The COMPASS experiment at CERN will directly access polarization of gluons in the nucleon in the region $x_g > 0.02$. It will use a polarized muon beam of 100 GeV and 200 GeV and longitudinally polarized hydrogen (NH_3) and deuterium (^6LiD) targets. The gluon polarization will be determined from the measurements of charmed meson production and from the production of correlated, high- p_t hadron pairs h^+h^- which tag the photon-gluon fusion reaction. In one year of data taking, the gluon polarization will be determined with a precision $\delta(\Delta G/G) \sim 0.15$ and 0.05 using the first and the second measurement, respectively.

PACS numbers: 12.39. -x, 13.20. Fc, 13.60. -r, 13.85. Ni

1. Introduction

How is the nucleon spin made out of partons?

The first answer came from the European Muon Collaboration, 10 years ago [1], and it indicated a problem; within the simple Quark-Parton Model (QPM), the quarks carry only a small fraction of the proton's spin. In the attempt to clarify the 'spin crisis', experiments were launched at CERN (SMC: [2], [3] and references therein), SLAC (E142 [4]; E143 [5], [6]; E154 [7]; E155 [8]) and DESY (HERMES [9]), using proton, deuteron and ^3He targets. They confirmed the original EMC conclusion with a greater precision and have also shown that the Bjorken sum rule [10] is fulfilled. There was a large progress in the interpretation of the experimental results. In particular

* Presented at the Cracow Epiphany Conference on Spin Effects in Particle Physics and Tempus Workshop, Cracow, Poland, January 9–11, 1998.

** This work has been supported by the Polish Committee for Scientific Research (KBN), grant 621/E-78/SPUB/P03/021/97.

the perturbative QCD (PQCD) corrections to the first moments of the spin dependent structure functions were calculated to 3rd order in α_s [11]. The QCD evolution of the spin dependent structure functions $g_1(x, Q^2)$ of nucleons were calculated in the NLO ([12–15]) in two renormalization schemes: Adler–Bardeen [13] and \overline{MS} [16].

The evidence is growing that the spin problem is due to gluons. It sounds familiar: more than 30 years ago, the quark ‘momentum crisis’ was also overcome with gluons. Polarized gluons enter the perturbative evolution of the spin-dependent structure functions $g_1(x, Q^2)$ and contribute to the scaling violations. One can determine polarized gluon distribution from PQCD fits of polarized parton distributions to the data. This method is known to work very well for the structure functions $F_2(x, Q^2)$ and yields consistent values of the gluon distributions $g(x, Q^2)$ [17]. However, g_1 are determined from the asymmetries of spin dependent cross sections which are much smaller and have larger relative errors. Therefore, the present spin-dependent structure function data do not constrain well enough the polarized gluon distributions

$\Delta g(x, Q^2)$. For the first moment, $\Delta G(Q^2) = \int_0^1 dx g(x, Q^2)$, the SMC fits to all the spin structure functions data yield $0.9 \pm 0.3(\text{exp.}) \pm (1.0)(\text{theor.})$ (AB scheme) [2] and those of the E143 yield $0.4_{-0.7}^{+1.0}(\text{stat.})_{-0.6}^{+0.9}(\text{syst.})_{-0.1}^{+1.1}(\text{theor.})$ (AB scheme) and $1.8_{-0.7}^{+0.6}(\text{stat.})_{-0.5}^{+0.4}(\text{syst.})_{-0.6}^{+0.1}(\text{theor.})$ (\overline{MS} scheme) [19] at $Q^2 = 1 \text{ GeV}$ and 5 GeV , respectively.

The COMPASS (“Common Muon and Proton Apparatus for Structure and Spectroscopy”) experiment [20] will determine gluon polarization from the measurements of asymmetries of the spin dependent cross sections which are sensitive to gluons in the leading order: they are given by the photon-gluon fusion. The polarized muons will be scattered on polarized proton and deuteron targets. The polarized photon-polarized gluon interactions will be tagged in two different ways; by the selection of the open charm production and by the selection of correlated, high- p_t hadron (h^+h^-) pairs.

For the sake of clarification it should be noted that the COMPASS collaboration has a broad physics program which will be carried using also proton and pion beams of 300 GeV (‘hadron program’). The hadron program includes central production of glueballs, single and double charmed baryons and Primakoff reactions. The experimental set-up will differ around the target region, while most of the spectrometers will be the same.

2. Overview of the methods

The virtual photon-gluon fusion (PGF) process is shown in Fig. 1. The basic process is the production of $q\bar{q}$ pair from virtual photon-gluon interaction, as shown in Fig. 2. The flux of polarized virtual photons is generated

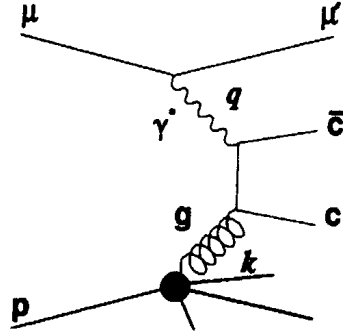


Fig. 1. The virtual photon-gluon fusion (PGF) diagram for the production of charm quarks. The COMPASS will use polarized muon beam and polarized protons (or deuterons) in the target. Therefore, both the virtual photons and the gluons will be polarized.

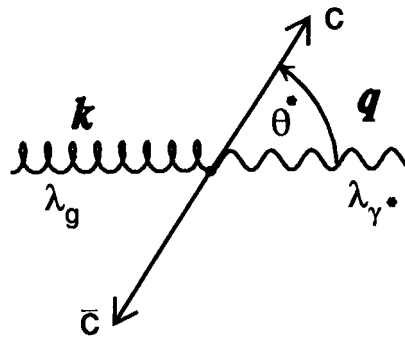


Fig. 2. The virtual photon-gluon scattering in their center of mass system. The virtual photon of the four-momentum q and the helicity λ_{γ^*} interacts with the gluon of the four momentum k and helicity λ_g to produce a pair of $q\bar{q}$ quarks. The angle of the c quark relative to the gluon direction is θ^* .

by the beam of polarized muons and the polarized gluons come from polarized nucleons in the target. The cross section for this process depends on the helicities of the virtual photon and the gluon, λ_{γ^*} and λ_g , respectively:

$$\sigma(\hat{s}, \cos \theta^*) = \sigma_0(\hat{s}, \cos \theta^*) + \lambda_{\gamma^*} \lambda_g \Delta\sigma(\hat{s}, \cos \theta^*). \quad (1)$$

The kinematics is defined in the virtual photon-gluon center of mass system. With the virtual photon and the gluon four-vectors q and k , respectively, the total energy is $\hat{s} = (q + k)^2 = -Q^2 + 2m\nu x_g$. Here we are using the deep inelastic scattering variables: $-Q^2 = q^2$, ν is the energy of virtual photon, x_g is the fractional momentum of a gluon in the proton and m is

the proton mass. The angle θ^* is the production angle of a quark relative to the gluon direction. In Eq. (1) the terms σ_0 and $\Delta\sigma$ are spin-independent and the spin-dependent cross sections, respectively. Both are functions of the kinematic variables and they will be discussed later.

The PGF process leads to the production of $q\bar{q}$ pair which could be either heavy $c\bar{c}$ charm quarks or light ($u\bar{u}$, $d\bar{d}$, $s\bar{s}$) quarks. In the COMPASS experiment both cases will be studied.

Neglecting contribution from the sea, the production of a charm quark (antiquark) is a background-free signature of the PGF. It will be tagged by the production of the charmed mesons, D^0 , \bar{D}^0 and $D^{*+}(2010) \rightarrow D^0\pi^+$. The charmed meson will be identified using hadrons from their decay, in particular $D^0(\bar{D}^0) \rightarrow K^-\pi^+$ ($K^+\pi^-$), where both hadrons will be identified with the RICH Cerenkov counters and their momentum vectors will be reconstructed in the magnetic spectrometers.

The tagging of the PGF leading to the production of light quark pairs requires strong suppression of background which comes from the leading order (LO) virtual photon-quark scattering ($\gamma^*q \rightarrow q$) and from the Compton process ($\gamma^*q \rightarrow qq$). It has been however demonstrated that background can be suppressed using cuts on the hadronic final states.

2.1. PGF model works well for unpolarized scattering

The PGF model has not been used yet in the analysis of polarized scattering data. However, in the unpolarized scattering, it is used to determine the unpolarized gluon distribution in the proton which agrees well with the one obtained from the NLO QCD fits to the data on structure function $F_2^p(x, Q^2)$. The most recent examples come from the preliminary ZEUS and H1 data from the HERA $e-p$ collider [17]. Figure 3 shows the reconstruction of D^0 and D^{*+} mesons from the invariant mass of $K\pi$ and from the difference of the invariant masses of $K\pi\pi$ and $K\pi$, respectively [18]. The same procedure will be used in the COMPASS experiment.

The method used for D^{*+} identification requires explanation. There is the sequential decay: $D^{*+} \rightarrow D^0\pi_s^+$ followed by $D^0 \rightarrow K^-\pi^+$. The difference of masses between D^{*+} and D^0 is 145 MeV. It is only 5 MeV above the mass of the pion π_s^+ and this pion has a small momentum in the D^{*+} rest mass system. Therefore the difference of the invariant masses $m(\pi_s^+\pi^+K^-) - m(\pi^+K^-)$ is usually more precisely determined than $m_{D^*} = m(\pi_s^+\pi^+K^-)$.

Figure 4 shows the gluon distribution obtained from unfolding of the next to leading order (NLO) PGF cross section for the D^{*+} production on the proton. It agrees well with the one obtained from the NLO QCD fits to the F_2^p data.

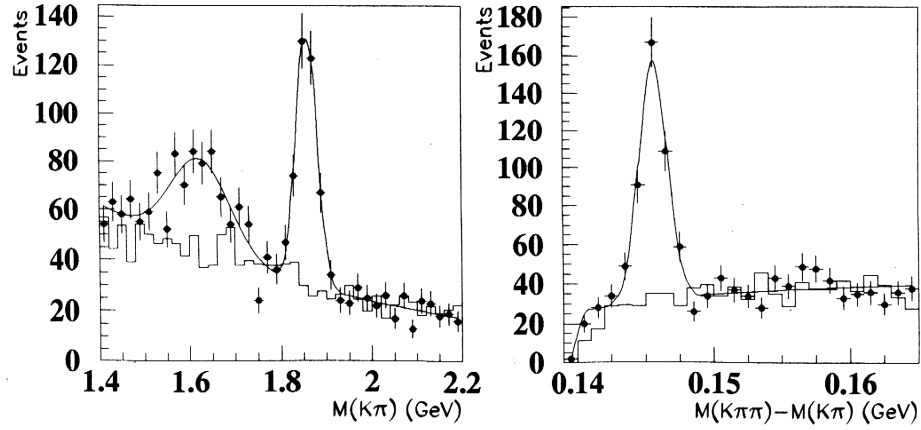


Fig. 3. Preliminary data from ZEUS (1995) at HERA [18]. The plot on the left shows $D^0 \rightarrow K\pi$ reconstructed from the invariant mass $M(K\pi)$. The plot on the right shows $D^{*+} \rightarrow D^0\pi^+$ reconstructed from the difference $M(K\pi\pi) - M(K\pi)$.

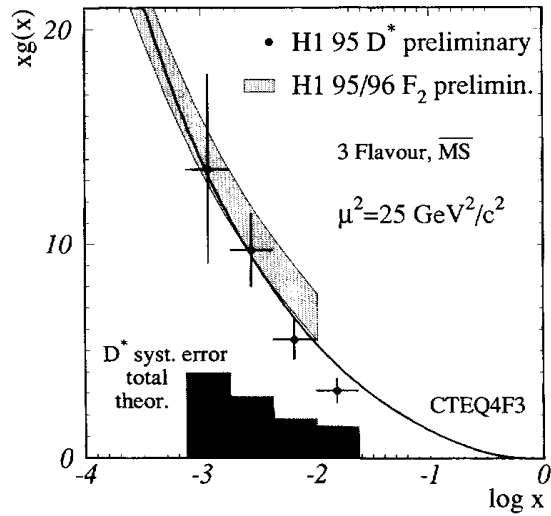


Fig. 4. The gluon distribution $xg(x)$ as a function of $\log x$. The data points were obtained from preliminary H1 (1995) data at HERA on D^{*+} production cross section and using the NLO PGF model calculations. The band shows the gluon distribution obtained from the NLO PQCD fits to the preliminary F_2^p data from 1995/96 (Ref. [17]).

2.2. Need of the NLO calculations for polarized PGF

There are several NLO calculations available for the unpolarized PGF model [21]. 'The K-factor', which is the ratio of the cross sections in NLO and LO, is known to be about 1.5.

For the polarized scattering there is only an approximate NLO calculation of $g_1^{c\bar{c}}$ of the proton for $Q^2 \geq 10 \text{ GeV}^2$ [22]. Figure 5 shows the comparison of the LO and approximate NLO predictions. The NLO effects are large and lead to a change of sign of $g_1^{c\bar{c}}$ at small x . However it is not clear what is expected at smaller values of Q^2 , which are relevant for the COMPASS experiment. There is clearly a need of such calculations.

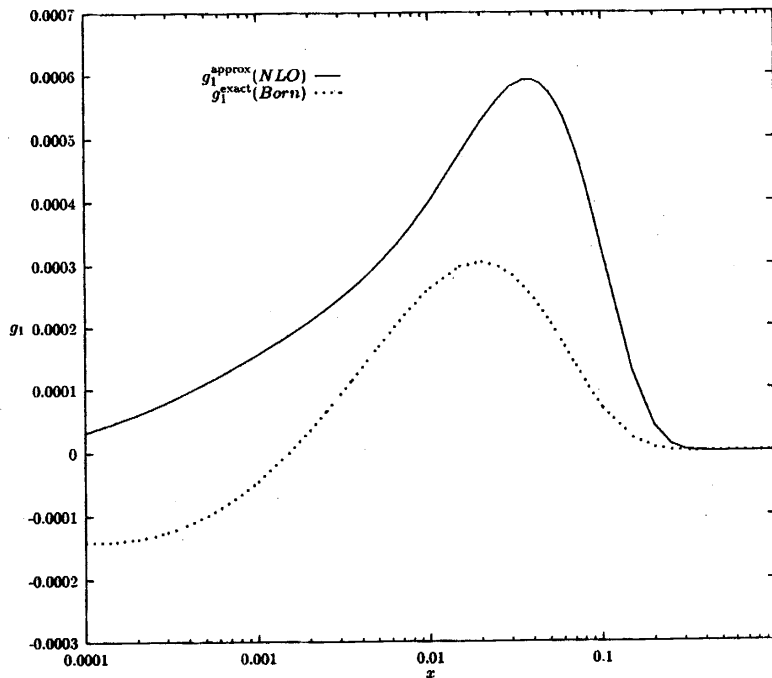


Fig. 5. The structure function $g_1^{c\bar{c}}$ from the LO (exact) and the NLO (approximate) calculations at $Q^2 = 10 \text{ GeV}^2$ (Ref. [22]).

2.3. Contribution from resolved photons is small

In the PGF, the production of $c\bar{c}$ is due to "direct" interaction of the virtual photon with the gluon. However, there is also a contribution from the "resolved photon" reactions, in which the virtual photon behaves as a

source of partons. In this case the $c\bar{c}$ production is due to the interaction between parton constituent of the virtual photon and the parton from the proton (mainly $gg \rightarrow c\bar{c}$). At small photon energies this contribution is expected to be below 4%, as seen in Fig. 6.

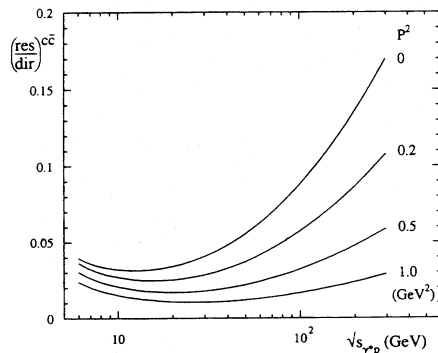


Fig. 6. The ratio of cross sections for $c\bar{c}$ production in resolved photon and direct photon interactions as a function of the total energy in γ^*p center of mass system (Ref. [23]). In the COMPASS experiment $\sqrt{s_{\gamma^*p}}$ will be in the range 8–13 GeV. The variable P^2 is the photon virtuality (Q^2).

3. The experimental setup for the muon program

The experiment will be set up on the muon beam line M2 from the SPS at CERN. It will occupy the location of the experiment NA47 of the SMC. The spectrometer lay out is shown in Fig. 7. Its basic concept is similar to that of the SMC but with several important modifications. They are due to five times higher beam intensity, larger acceptance, identification of charged hadrons and to measurement of neutral pions.

3.1. The spectrometer

The incoming muons and also the scattered muons and hadrons produced under small angles will be measured in scintillating fibre tracking detectors. Outside of the beam region the tracking will be done using wire chambers. In order to provide large acceptance for charged hadrons, the spectrometer will have two stages.

The first stage will have the angular acceptance of ± 200 mrad which will be matched by a new superconducting solenoid of the polarized target. The spectrometer magnet will have a large aperture and the bending power of 1 Tm. Its purpose is to measure small momentum hadrons at large angles.

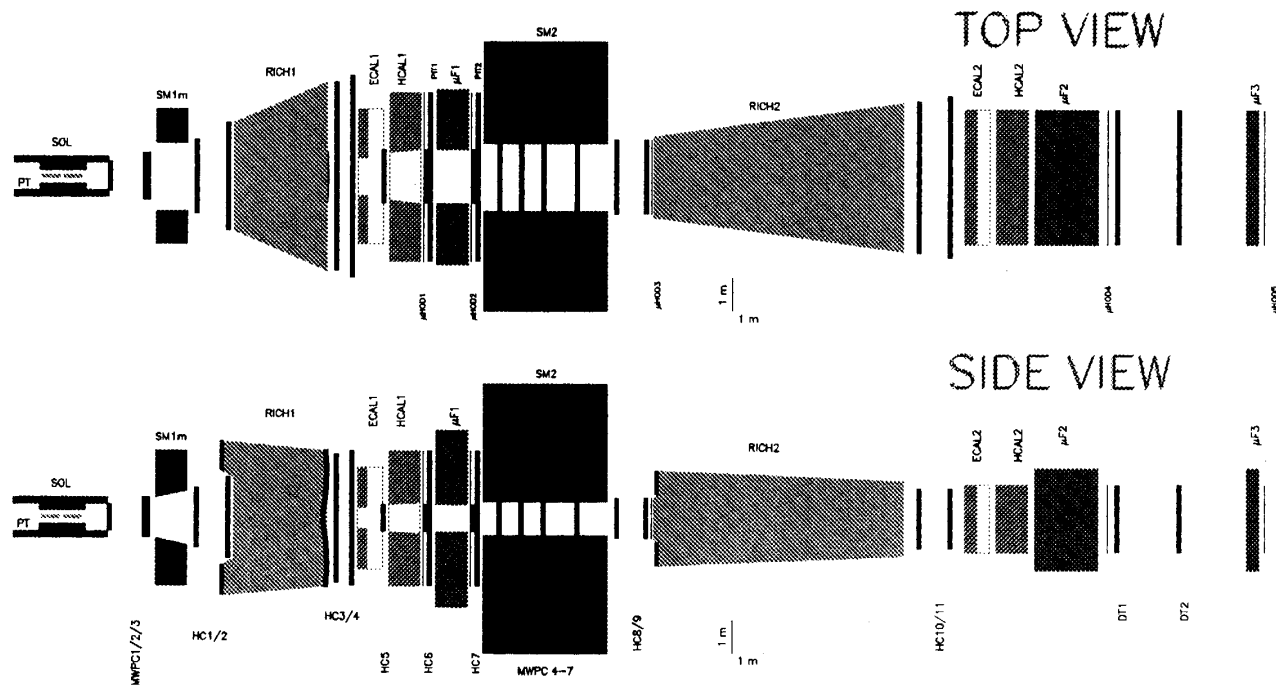


Fig. 7. The COMPASS spectrometer. The muon beam comes from the left and hits the polarized target (PT) inside the superconducting solenoid (SOL). The scattered muon and the produced hadrons are measured and identified in the two-stage spectrometer: SM1(2) are the spectrometer magnets; RICH1(2) are Cherenkov counters, ECAL1(2) and HCAL1(2) are electromagnetic and hadronic calorimeters, respectively; $\mu F1$ -3 are muon filters; MWPC1-7, HC1-11, PIT1-2 and DT1-2 are tracking detectors; $\mu HOD1$ -5 are trigger hodoscopes.

The purpose of the second stage is to measure the scattered muons and charged hadrons of high momentum. The SMC magnet will provide the bending power of 2 Tm. Each spectrometer stage will be equipped with the ring-imaging Cherenkov counter (RICH). They will be filled with different gases to provide $\pi - K$ separation in the momentum interval 3–65 GeV and 30–120 GeV, respectively. Each spectrometer stage will also be equipped with lead-glass calorimeters to measure neutral pions.

The scattered muon will be identified as a particle penetrating an iron wall downstream of the second spectrometer. Behind the iron wall there will be tracking chambers and trigger hodoscopes. The muon filter in the first stage will be used in the hadron program.

3.2. The polarized targets

The targets will be polarized using the same technique as in the SMC experiment [24]. The polarized target is shown in Fig. 8. The data will be taken with polarized protons and deuterons.

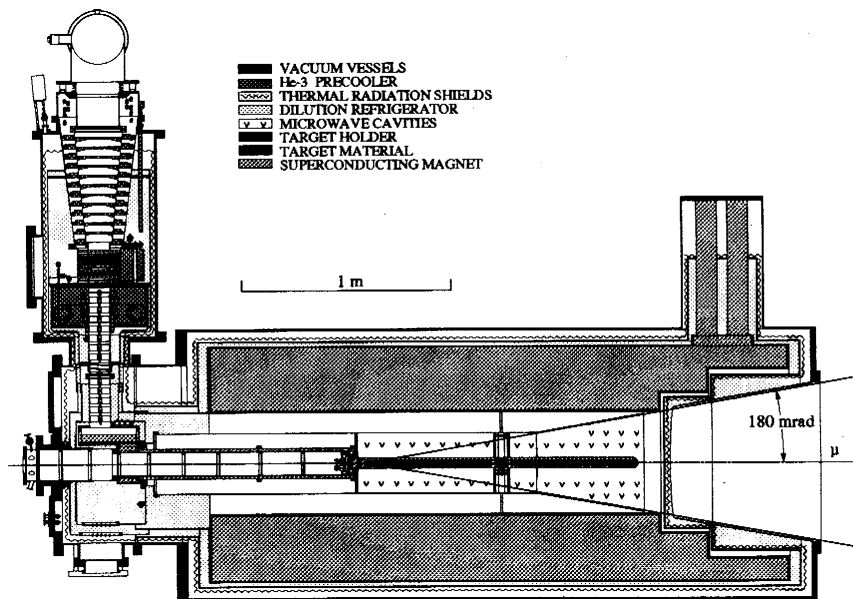


Fig. 8. Polarized target setup of the COMPASS experiment.

In the first case the target material will be ammonia (NH_3), where the protons can be polarized to about 85% and the fraction of the polarizable target material (the dilution factor) is $f = 0.18$.

In the second case lithium deuteride (${}^6\text{LiD}$) will be used. It can be polarized to 50% and it has a dilution factor of $f = 0.5$.

The target material will be contained in two identical target cells where it will be polarized in opposite directions, parallel and antiparallel to the beam. The length of each target cell will be 60 cm and its diameter 3 cm.

3.3. The luminosity

The beam energy will be 100 GeV and/or 200 GeV. Its polarization has been measured at both energies by the SMC [3] and it is about 80%.

The beam intensity will be about $10^8/\text{s}$ during spills of 2.4 s which are repeated every 14.4 sec. With the ammonia target the luminosity will be $\mathcal{L} = 4.3 \cdot 10^{37} / \text{cm}^2/\text{day} = 43/\text{pb}/\text{day}$.

4. $\Delta G/G$ from $c\bar{c}$ production

4.1. The cross section for virtual photon charm photoproduction

The cross section for the process $\mu p \rightarrow c\bar{c}X$ is written as a product of the flux of virtual photons and of the cross section for the process $\gamma^* p \rightarrow c\bar{c}X$:

$$\frac{d^2\sigma^{\mu p \rightarrow c\bar{c}X}}{dx dQ^2} = \Gamma(E_\mu, Q^2, \nu) \sigma^{\gamma^* p \rightarrow c\bar{c}X}(Q^2, \nu). \quad (2)$$

The virtual photon flux is given by:

$$\Gamma(E_\mu, Q^2, \nu) = \frac{\alpha_e}{2\pi Q^2} \frac{2(1-y) + y^2 + \frac{Q^2}{2E_\mu^2}}{(Q^2 + \nu^2)^{1/2}}, \quad (3)$$

where α_e is the electromagnetic coupling constant and $y = \nu/E_\mu$. The flux increases at small Q^2 and is largest at $Q_{\min}^2 = m_\mu^2 y^2 / (1-y)$. Therefore the virtual photon beam is quasi-real. It should be noted that the energy scale of the process $\gamma^* q \rightarrow c\bar{c}$ is not Q^2 but $\hat{s} \geq 4m_c^2$.

The virtual photon cross section is written as a product of the cross section for the photoproduction of charm by real photons, $\gamma p \rightarrow c\bar{c}X$, and of a dipole form factor term:

$$\sigma^{\gamma^* p \rightarrow c\bar{c}X}(Q^2, \nu) = \frac{\sigma^{\gamma p \rightarrow c\bar{c}X}(\nu)}{\left(1 + \frac{Q^2}{15.2 \text{GeV}^2}\right)^2}. \quad (4)$$

The photoproduction cross sections have been measured by several experiments and their results are shown in Fig. 9. In this figure are shown also

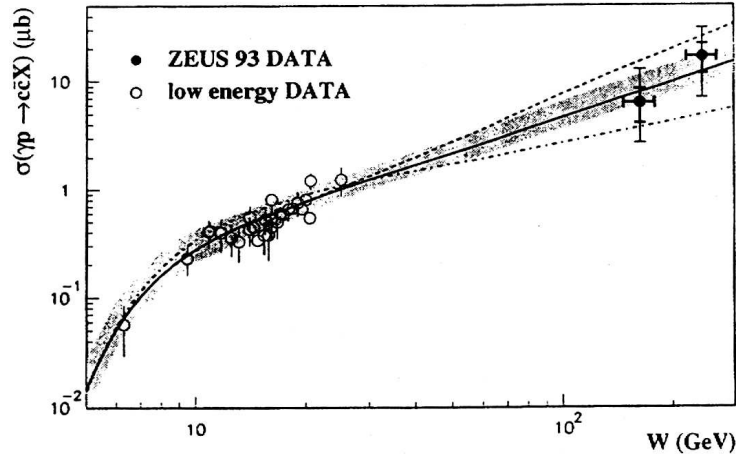


Fig. 9. The total $c\bar{c}$ photoproduction cross sections as a function of W , the total energy in γ^*p center of mass system. The inner error bars represent the statistical errors and the outer ones the systematic errors. The solid line shows the NLO prediction (Ref. [25]).

the NLO predictions which use unpolarized gluon distributions $g(x_g)$ as an input. Predictions agree well with the data.

In the COMPASS experiment, the data used for the analysis of $\Delta G/G$ from production of charm will be collected at 100 GeV beam energy and will cover virtual photon energy range of $35 < \nu < 85$ GeV. In this range, the muon cross section is $\sim 0.5 \mu\text{b}$ and the charm production cross section is ~ 2 nb (0.4%). The amount of data collected per day will therefore be: 20M of all events and 82k of $c\bar{c}$ events.

4.2. The measured asymmetry

The COMPASS experiment will measure the asymmetry of the production rate of charmed events from targets which are polarized in opposite direction ($\overleftrightarrow{\hat{e}}$):

$$A_{\text{meas}}^{\mu p \rightarrow c\bar{c}} = \frac{N_{c\bar{c}}^{\overleftarrow{\hat{e}}} - N_{c\bar{c}}^{\overrightarrow{\hat{e}}}}{N_{c\bar{c}}^{\overleftarrow{\hat{e}}} + N_{c\bar{c}}^{\overrightarrow{\hat{e}}}}. \quad (5)$$

The direction of the muon polarization is shown with the upper arrow and it does not change during data taking. This asymmetry is smaller than the asymmetry of the corresponding cross sections for the absorption of virtual photons:

$$A_{\text{meas}}^{\mu p \rightarrow c\bar{c}} = A^{\gamma^* \rightarrow c\bar{c}} D P_B P_T f. \quad (6)$$

Here $P_{B(T)}$ are beam (target) polarizations, f is the dilution factor of target material and D is the depolarization factor which accounts for the polarization transfer from the muon to the virtual photon:

$$D(y) \simeq \frac{1 - (1 - y)^2}{1 + (1 - y)^2}. \quad (7)$$

At larger values of y virtual photons are more polarized.

Taking the beam polarization of 0.8, an average depolarization factor of 0.55, and the ammonia target, which is polarized to 0.85 and has the dilution factor of 0.18, the measured asymmetry is reduced by a factor of 0.07 relative to the virtual photon asymmetry.

4.3. The virtual photon asymmetry in the PGF model

Using Eq. (1) the virtual photon asymmetry can be written in terms of the PGF model:

$$A^{\gamma^* p \rightarrow c\bar{c}} = \frac{\Delta\sigma^{\gamma^* p \rightarrow c\bar{c}}}{\sigma^{\gamma^* p \rightarrow c\bar{c}}} = \frac{\int_{-1}^1 d\cos\theta^* \int \frac{2m\nu}{4m_c^2} \Delta\sigma(\hat{s}, \cos\theta^*) \Delta G(x_g, \hat{s})}{\int_{-1}^1 d\cos\theta^* \int \frac{2m\nu}{4m_c^2} \sigma_0(\hat{s}, \cos\theta^*) G(x_g, \hat{s})}. \quad (8)$$

The cross sections $\Delta\sigma(\hat{s}, \cos\theta^*)$ and $\sigma_0(\hat{s}, \cos\theta^*)$ for the process $\gamma^* g \rightarrow c\bar{c}$ are known in the LO [26] and the NLO [27], respectively. In the LO, after the integration over $\cos\theta^*$, they are:

$$\Delta\sigma(\hat{s}) = \frac{4}{9} \frac{2\pi\alpha_e\alpha_s}{\hat{s}} \left[3\beta - \ln \frac{1+\beta}{1-\beta} \right] \quad (9)$$

and

$$\sigma_0(\hat{s}) = \frac{4}{9} \frac{2\pi\alpha_e\alpha_s}{\hat{s}} \left[-\beta(2-\beta)^2 + \frac{1}{2}(3-\beta^4) \ln \frac{1+\beta}{1-\beta} \right]. \quad (10)$$

Here $\beta = (1 - 4m_c^2/\hat{s})^{1/2}$ is the velocity of the charm quarks in their center of mass system (their Lorentz factor is $\gamma = \hat{s}/(2m_c)$) and α_s is the strong coupling constant.

The ratio $\Delta\sigma/\sigma_0$ is written as $a_{LL} \equiv \Delta\sigma/\sigma_0$. The virtual photon asymmetry can be approximated by the expression:

$$A^{\gamma^* p \rightarrow c\bar{c}} \simeq \left\langle a_{LL}^{\gamma^* g \rightarrow c\bar{c}} \cdot \frac{\Delta G}{G} \right\rangle, \quad (11)$$

which shows that in order to have a large virtual photon asymmetry, an overlap of non-zero values of a_{LL} and of $\Delta G/G$ is required.

4.4. The kinematic region of the measurements

Figure 10 shows the unpolarized and the polarized gluon distributions as given by the parameterizations from Ref. [28]. The gluon polarization, $\Delta g/g$, is expected to be large at $x_g \simeq 0.1$.

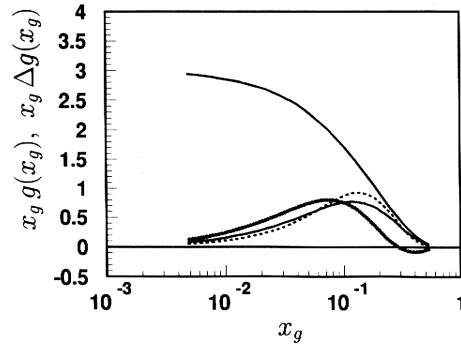


Fig. 10. Distributions of unpolarized and polarized gluons given by parameterizations of Ref. [28]. The upper curve shows $x_g g(x_g)$ and the lower three curves correspond to different parameterizations of $x_g \Delta g(x_g)$.

Figure 11 shows the cross sections σ_0 and $\Delta\sigma$ for the interactions $\gamma^* g \rightarrow c\bar{c}$. The largest values of a_{LL} are expected for $\hat{s} \simeq 13 \text{ GeV}^2$.

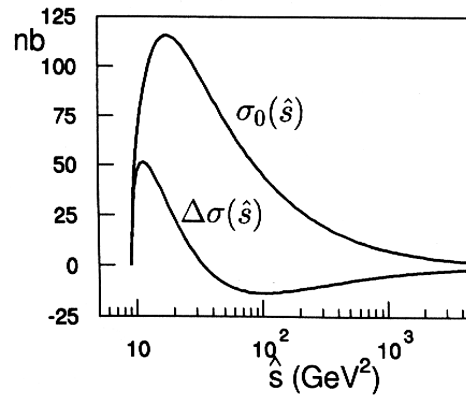


Fig. 11. The cross sections σ_0 and $\Delta\sigma$ for the interaction $\gamma^* g \rightarrow c\bar{c}$ as a function of the total energy \hat{s} .

These values of x_g and of \hat{s} lead to $\nu = \hat{s}/(2m x_g) = 65 \text{ GeV}$. Therefore for the muon beam of energy $E_\mu = 100 \text{ GeV}$, the value of $y = \nu/E_\mu$ will be 0.65 for which the depolarization factor is large: $D = 0.8$. These regions will

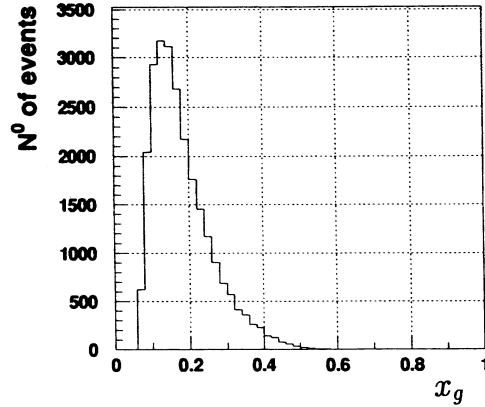


Fig. 12. Distribution of x_g in COMPASS experiment, from $c\bar{c}$ production by the PGF using virtual photons of energy $35 < \nu < 85$ GeV.

be covered in the COMPASS experiment, where $35 < \nu < 85$ GeV. Fig. 12 shows the Monte-Carlo simulation of the coverage of x_g which extends down to 0.07.

Running with 200 GeV muons COMPASS will access smaller values of x_g (by about a factor of two) where, however, the measured asymmetry is expected to be smaller.

4.5. Fragmentation $c(\bar{c}) \rightarrow D^0(\bar{D}^0)$

Figure 13 shows the mesonic and baryonic “strings” which fragment into charmed mesons and baryons, and Fig. 14 gives predictions [29] for the production probability of dominant final states using the Lund string fragmentation model [30]. The expected yield of D^0 and \bar{D}^0 per $c\bar{c}$ event is 1.2.

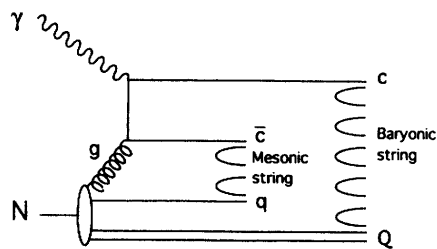


Fig. 13. Strings which contribute to the hadronization of $c\bar{c}$ into charmed hadrons [29].

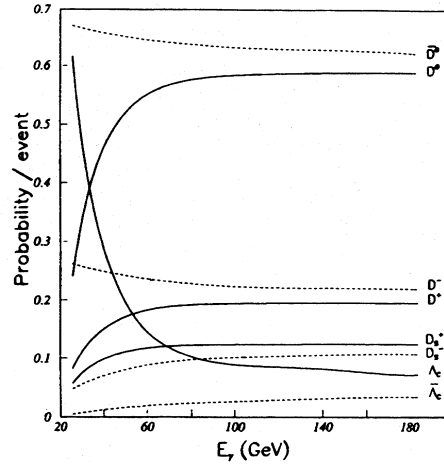


Fig.14. Predictions for the probability of charmed hadron production per $c\bar{c}$ event [29].

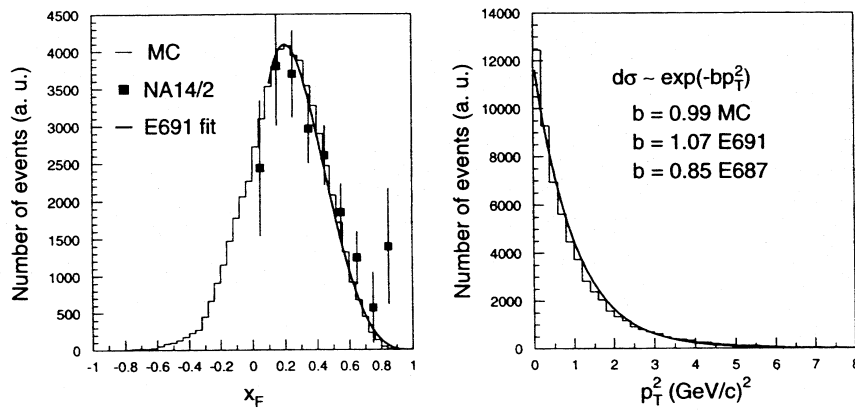


Fig. 15. Distributions of x_F and p_t^2 of D^0 mesons from the data and from the Monte Carlo simulation (shown as a histogram).

Figure 15 shows that data on charmed meson photoproduction [29] are well reproduced by Monte Carlo using AROMA [31] and JETSET [32] event generators.

In the COMPASS experiment the charmed mesons D^0 and \bar{D}^0 will be identified by their decay into hadronic states. “The golden” decay channel:

$$D^0(c\bar{u}) \rightarrow K^-\pi^+,$$

$$\bar{D}^0(\bar{c}u) \rightarrow K^+\pi^-$$

has the branching ratio of 0.04. The hadrons will be identified and their momentum vectors will be reconstructed. However their decay vertex will not be determined due to scattering of hadrons in the target. The reconstruction program will assign them to the muon interaction vertex, together with all charged hadrons produced in the muon interaction.

The combinatorial background from “wrong” $K\pi$ pairs can significantly increase the error on the virtual photon asymmetry:

$$\delta A = \frac{1}{P_B P_T f D} \frac{1}{N_S^{1/2}} \left(1 + \frac{N_B}{N_S} \right)^{1/2}. \quad (12)$$

Here $N_{S(B)}$ is the number of correct (background) associations. The expected resolution in the invariant mass of $K\pi$ is about 10 MeV. In the mass window ± 20 MeV around D^0 mass, the signal is largely dominated by background; Monte Carlo studies show that the expected signal to background ratio is $N_S : N_B = 1 : 30$. This huge background has to be suppressed to an acceptable level.

4.6. Background reduction

The background is suppressed with kinematics cuts on two variables: $z_D = E_D/\nu$, where E_D is energy of D^0 in the laboratory system and on $\cos\theta_K^*$, where θ_K^* is the angle of K^0 in rest system of D^0 relative to D^0 direction in the laboratory system.

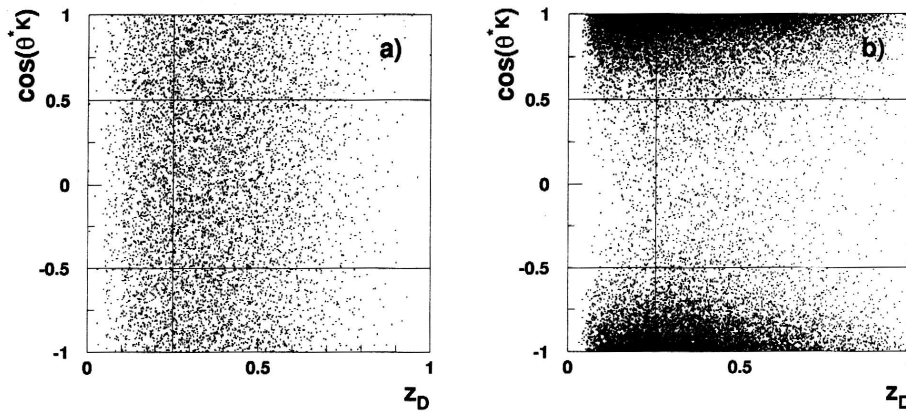


Fig. 16. Distributions of events as a function of $\cos\theta_K^*$ and z_D for (a) K^0 decays and (b) the combinatorial background.

Figure 16 shows the distribution of signal and background events on the plane $(\cos\theta_K^*, z_D)$. The signal events have a uniform distribution in $\cos\theta_K^*$, while the background ones populate mostly forward and backward directions. This difference is due to p_t : in D^0 decay $p_{t_{\max}} = 0.86$ GeV which is larger than the transverse momentum from soft hadronisation of first rank hadrons. Therefore random association of these hadrons will lead to collinear “decays”.

In the window defined by $z_D > 0.25$ and $|\cos\theta_K^*| < 0.5$ there is 29% of signal events but only 2.5% of background events. Using this window and also the mass window of ± 20 MeV and $35 < \nu < 85$ GeV the signal-to-background ratio becomes $N_S : N_B = 1 : 3.9$ and the number of D^0 events per day will be ~ 880 .

4.7. The expected precision of $\Delta G/G$

After two years of data taking, which will be shared between NH_3 and ${}^6\text{LiD}$ targets (1:1.5), the expected number of golden events after the cuts is 66k. With 250k background events it leads to the error on the virtual photon asymmetry of $\delta A^{\gamma^* p \rightarrow c\bar{c}} = 0.076$.

There are two ways to increase the precision of $\Delta G/G$: to select events with D^{*+} and to use events coming from the kinematics region where the asymmetry a_{LL} is bigger.

The golden sample contains D^0 from direct fragmentation of charm quarks and also from the decay $D^{*+} \rightarrow D^0 \pi_s^+$, which has a 2.7% branching ratio. The identification of D^{*+} decays has already been discussed. It has been pointed out (sect. 2.1) that this channel has small combinatorial background. In order to select D^{*+} from the distribution $m(K\pi\pi) - m(K\pi)$ one can use narrower mass window, $\Delta m = \pm 5$ MeV. Also cuts on z_D and on $\cos\theta_K^*$ will be less restrictive: $z_D > 0.2$ and $|\cos\theta_K^*| < 0.85$. The expected rate is 300 D^{*+} events per day. The resulting error on the asymmetry combined with that obtained from the remaining golden sample is

$$\delta A^{\gamma^* p \rightarrow c\bar{c}} = 0.051 \quad (13)$$

which leads to:

$$\delta \left(\frac{\Delta G}{G} \right) = 0.14. \quad (14)$$

Figure 17 shows the expected asymmetries in $c\bar{c}$ production from virtual photon and from muon interactions together with the expected experimental errors. Relative to the muon asymmetry, the measured one will be suppressed by a factor of 0.12 coming from beam and target polarizations and from the dilution factor (Eq. (6)).

The asymmetry $a_{LL}(\hat{s}, \cos \theta^*)$ increases for smaller values of θ^* . Small θ^* corresponds to small transverse momenta of D^0 relative to virtual photon direction. It has been shown that for events with $p_t^D < 1$ GeV the error will be significantly smaller:

$$\delta \left(\frac{\Delta G}{G} \right) = 0.11. \quad (15)$$

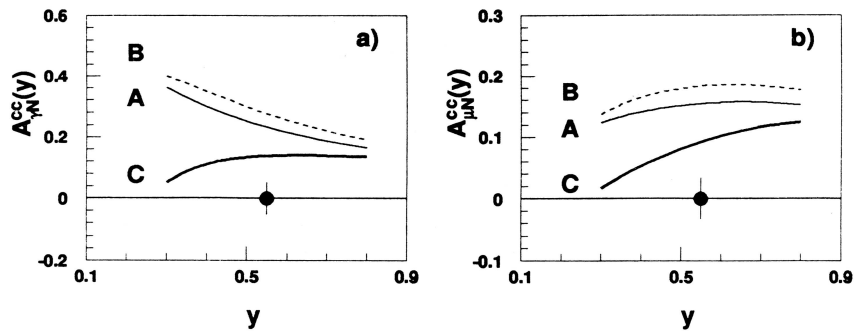


Fig.17. The asymmetry (a) $A_{\gamma^* p}^{c\bar{c}}$ and (b) $A_{\mu p}^{c\bar{c}}$ for charmed meson production as a function of y . The curves correspond to three different parameterizations of $\Delta g(x_g)$ from Ref. [28]. The precision of measurements in the range $0.35 < y < 0.85$ is indicated by the error bars of the data points plotted at $A = 0$.

5. $\Delta G/G$ from light $q\bar{q}$ production

It has been shown in Ref. [34] that $\Delta G/G$ can be determined from the PGF leading to light $q\bar{q}$ production. The beam energy will be 200 GeV, which is higher than for $c\bar{c}$ production, but still too small to have clear hadronic jets ($\hat{s} \sim 40$ GeV²). Therefore, the minimum requirement is to have at least two hadrons in the final state ($h_1 h_2$). The light quark production from PGF has a large background due to the LO fragmentation and the Compton scattering. However, the Monte Carlo studies show that the background can be suppressed to a tolerable level. These studies were made with LEPTO [33], PYTHIA [32] and POLDIS [35] generators.

5.1. The background

Figure 18 shows the signal and also the background processes, which are due to the LO virtual photon-quark scattering ($q\gamma^* \rightarrow q$) and the Compton process ($q\gamma^* \rightarrow qg$).

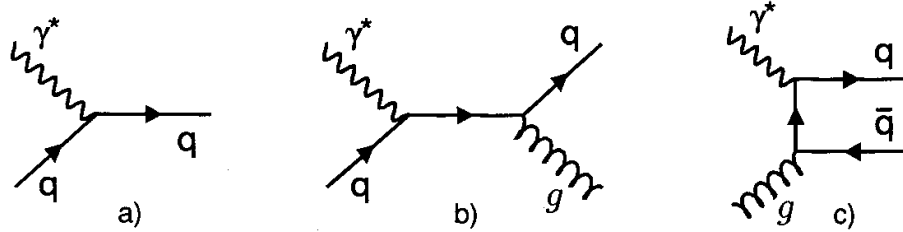


Fig. 18. Lowest order diagrams for γ^*p interactions: (a) virtual photo-absorption, (b) gluon radiation (Compton diagram) and (c) virtual photon-gluon fusion (PGF).

5.2. Background reduction

The following cuts will be used to (practically) eliminate the LO background (cuts 1–3) and to suppress the Compton background (cuts 4 and 5):

1. $p_T^{h_1(h_2)} > 1 \text{ GeV}$ and $m_{h_1, h_2} > 2.5 \text{ GeV}$; this cut is equivalent to a cut on \hat{s} ,
2. $z_{h_1(h_2)} > 0.1$; this cut largely eliminates hadrons from the target fragmentation,
3. $\phi_{h_1(h_2)} = 180^\circ \pm 30^\circ$,
4. h^+h^- pair; it enhances fragmentation from $q\bar{q}$,
5. K^+K^- pair; it enhances fragmentation from $s\bar{s}$.

Before cuts, signal to background ratio is S:B=1:7. The relative contribution of the LO, Compton and PGF processes is shown in Fig. 19. In the same figure are shown also these contributions after cuts:

- 1–3: the sample is reduced by $3.8 \cdot 10^{-2}$ and S:B=0.9:1 (Fig. 19(a)),
- 4: the sample is reduced by $1.4 \cdot 10^{-3}$ and S:B=1.1:1 (Fig. 19(b)),
- 5: the sample is reduced by $2.2 \cdot 10^{-4}$ and S:B=2:1 (Fig. 19(c)).

It can be seen that already after cuts 1–3, the LO contribution is largely suppressed and the ones from the PGF and the Compton are comparable. Further relative enhancements of the PGF can be obtained with cut 5, which however strongly reduces the event sample.

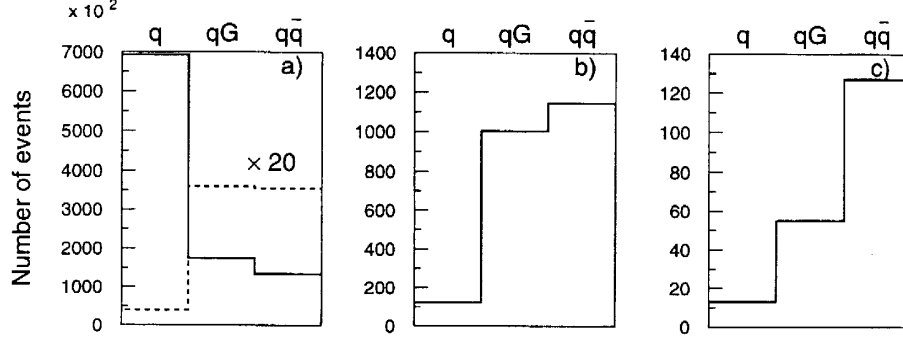


Fig. 19. Contribution of the virtual photo-absorption (q), Compton (qG) and PGF ($q\bar{q}$) to the cross section [34]: (a) no cuts (full line) and cuts 1–3 (dashed line), (b) h^+h^- pairs (cuts 1–4) and (c) K^+K^- pairs (cuts 1–5). Event numbers correspond to 10^6 generated events.

5.3. The contribution from Compton scattering

The Compton contribution (COM) gives also rise to the asymmetry which is different from the one of the PGF; both of them contribute to the measured asymmetry:

$$A^{\mu p \rightarrow h_1 h_2 X} \simeq \langle D \cdot a_{LL}^{\text{PGF}} \rangle \frac{\Delta G}{G} \frac{\sigma^{\text{PGF}}}{\sigma^{\text{TOT}}} + \langle D \cdot a_{LL}^{\text{COM}} \rangle A_1 \frac{\sigma^{\text{COM}}}{\sigma^{\text{TOT}}}. \quad (16)$$

Here $A_1 \simeq g_1/F_1$ is the virtual photon asymmetry and $\sigma^{\text{TOT}} = \sigma^{\text{PGF}} + \sigma^{\text{COM}}$ is the sum of muon cross section for PGF and Compton scattering. The asymmetries $a_{LL} \cdot D$ are shown in Fig. 20. The asymmetry for the PGF is large and negative and it weakly depends on $\cos \theta^*$, whereas the asymmetry for the Compton is positive and has a strong dependence on $\cos \theta^*$.

Therefore, the muon asymmetry given by Eq. (16) is the weighted sum of the two effects which are opposite in sign.

5.4. The determination of the kinematic variables

It has been shown [34] that the variable $\cos \theta^*$ can be reconstructed from hadron angles alone:

$$\cos \theta^* = \frac{\tan \theta^+ - \tan \theta^-}{\tan \theta^+ + \tan \theta^-}, \quad (17)$$

where $\theta^{+(-)}$ is the angle between hadron $h^{+(-)}$ and the virtual photon, in the laboratory system.

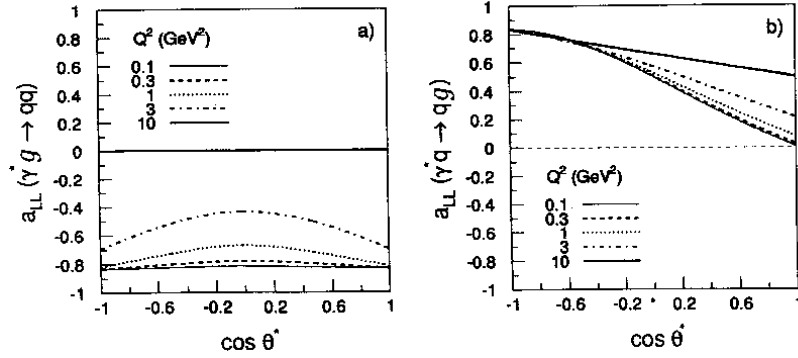


Fig. 20. Asymmetries $a_{LL} \cdot D$ for (a) PGF and (b) Compton process as a function of the quark production angle θ^* and for different values of Q^2 [34]. The center of mass energy is $\hat{s} = 10 \text{ GeV}^2$ and $y = 0.7$.

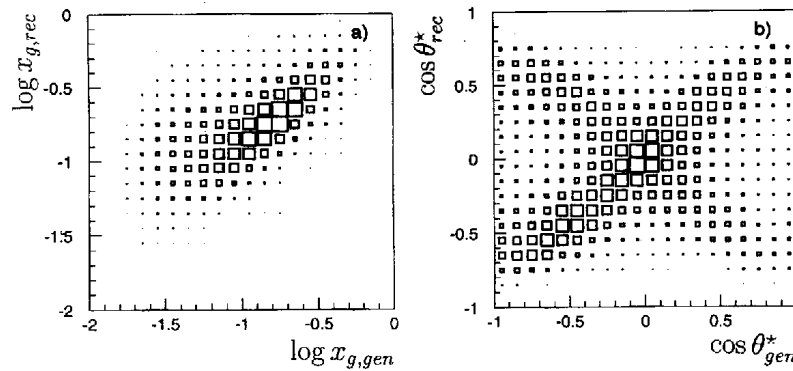


Fig. 21. Correlation between the generated and the reconstructed values of parton variables (a) x_g and (b) $\cos \theta^*$ [34]. The value of $\cos \theta^*$ is reconstructed using hadron kinematics only while x_g is obtained from both muon and hadron kinematic variables.

The variables \hat{s} and x_g can be reconstructed using both muon and hadron kinematics:

$$\hat{s} = \nu^2 \tan \theta^+ \tan \theta^-, \quad x_g = \frac{\hat{s} + Q^2}{2m\nu}. \quad (18)$$

Figure 21 shows the correlation between the true and the reconstructed values of x_g and $\cos \theta^*$ obtained with Monte Carlo simulation. In the case of Compton process, x_g should be taken as the fraction of proton's momentum carried by quark. In the second case the band at -45° is due to the definition of the angle: the hadron angle is defined for the positive hadron and there are two hadrons of opposite charge per event.

5.5. The range of x_g

Figure 22 shows the range of x_g and its coverage by events from the PGF and from the Compton process. It is seen that the Monte Carlo data covers $x_g > 0.02$. For the h^+h^- selection, contributions from both processes are similar, but PGF events are shifted to smaller x_g . For K^+K^- , as we have already discussed, the Compton contribution relative to that from PGF is suppressed by a factor of two.

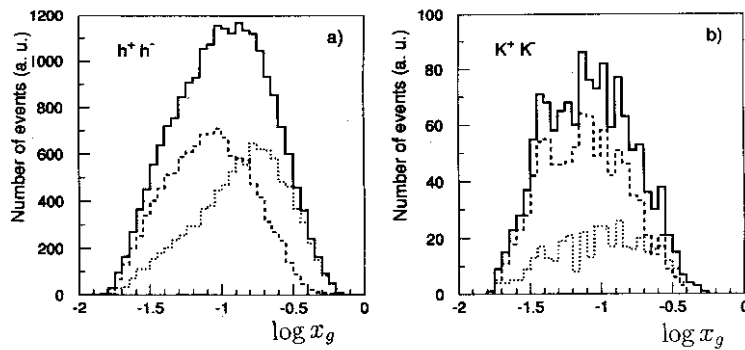


Fig. 22. Distributions of x_g for gluons from PGF (dashed line) and quarks from Compton process (dotted line) for (a) high p_t h^+h^- pairs and (b) K^+K^- pairs [34]. The full line is the sum of both. In the case of Compton process, x_g should be taken as the fraction of proton's momentum carried by quark.

5.6. The expected sensitivity

Figure 23 shows the muon asymmetry as a function of x_g for h^+h^- and K^+K^- selections, separately. In each case the predictions are shown for two different inputs of gluon polarizations. The difference between the solid and dashed curves accounts for the smearing of parton kinematics due to hadronisation. The error bars at the solid and open symbols correspond to the accuracy expected from 700k h^+h^- and 70k K^+K^- events obtained after one year of running with the ${}^6\text{LiD}$ target.

The important feature of the above predictions is a change of sign of the asymmetries; it is negative at small x_g , where PGF dominates and it becomes positive at high x_g , dominated by Compton process. Therefore negative asymmetry is a signature of positive gluon polarization.

In order to determine $\Delta G/G$, Compton contribution has to be subtracted from the measured asymmetry. The corresponding error will be dominated by the uncertainties in the ratio of cross sections, $\sigma^{\text{PGF}}/\sigma^{\text{COM}}$. The expected

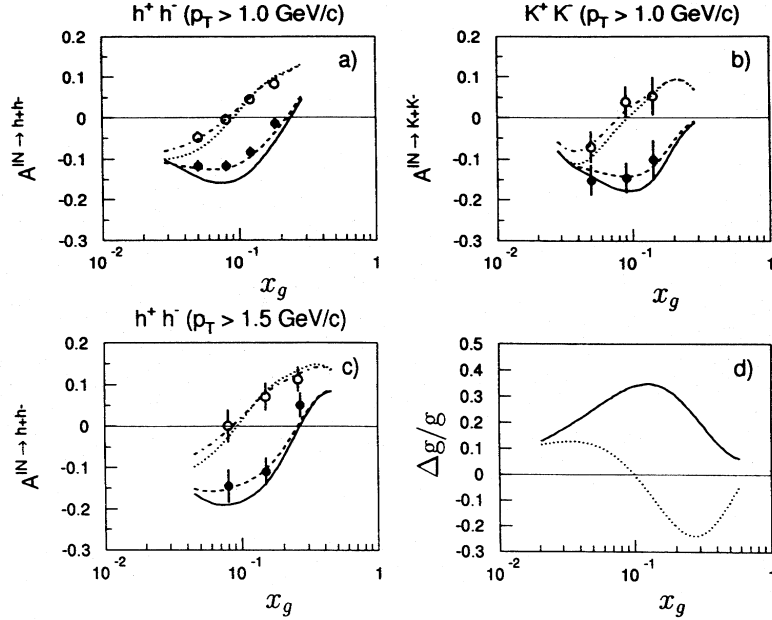


Fig. 23. The muon cross section spin-asymmetries $A^{\mu p \rightarrow h^+ h^- X}$ of Ref. [34] for (a) $h^+ h^-$ of $p_t > 1 \text{ GeV}$, (b) $K^+ K^-$ of $p_t > 1 \text{ GeV}$, (c) $h^+ h^-$ of $p_t > 1.5 \text{ GeV}$ as a function of $x_{g,\text{rec}}$ using two sets of polarized gluon distributions from Ref. [28] at $Q^2 = 10 \text{ GeV}^2$, shown in (d): set A — full line and full circles, set B — dotted line and open circles. The error bars indicate the relative statistical precision for one year of measurements. The full and dotted lines in (a)–(d) correspond to the true values of x_g while dashed and dot-dashed lines correspond to x_g reconstructed using hadron and muon kinematic variables.

resolution is:

$$\delta \left(\frac{\Delta G}{G} \right) = 0.05. \quad (19)$$

6. Other physics items of the muon program

The determination of $\Delta G/G$ is the main physics item of the “muon program” of COMPASS. There are, however, other items which can be studied using the same data sample, *i.e.* events from deep inelastic scattering of polarized muons on longitudinally polarized hydrogen and deuterium targets:

- Spin dependent structure functions $g_1^p(x, Q^2)$, $g_1^d(x, Q^2)$ determined from inclusive interactions and spin distribution functions of valence and sea quarks, $\Delta u_v(x, Q^2)$, $d_v(x, Q^2)$, $\bar{q}(x, Q^2)$ determined from both

inclusive and semi-inclusive interactions. New data will substantially increase the precision of the existing determinations. It is needed *e.g.* for the analysis of data from polarized proton interactions in RHIC.

- Longitudinal polarization of Λ^0 and its dependence on the direction of target polarization. It has not been measured yet.
- Spin dependent fragmentation functions of quarks into Λ^0 : $D_q^{+\Lambda}$ and $D_q^{-\Lambda}$, where $+(-)$ refers to spin of Λ which is parallel (antiparallel) to the quark spin. There is no data on spin-dependent fragmentation functions.

There are also interesting physics subjects which can be studied using transversely polarized protons and/or deuterons:

- Spin dependent structure functions $g_2^p(x)$ and $g_2^d(x)$. At present these evaluations have large statistical errors.
- Transversity $h_1(x)$ from semi-inclusive interactions. There is no data on this subject.

7. Other experiments planning to determine $\Delta G/G$

The HERMES collaboration at DESY is upgrading their detector in order to investigate electroproduction of D^0 and of J/ψ . The gluon polarization will be determined at around $x_g = 0.3$. After one year of data taking the accuracy will be $\delta(\Delta G/G) = 0.45$. Data taking will begin in 1999 [36].

At RHIC in BNL gluon polarization will be determined by STAR and PHENIX collaborations [37], using polarized p - p interactions at $\sqrt{s} = 200$ GeV. The studied reaction channels will include direct single photon production and inclusive single jet and di-jet production. The gluon polarization will be determined for $x_g < 0.1$. It is expected to have polarized protons in the year 2000 and the first spin physics runs will be possible in 2001.

Polarized proton option at HERA [38] is under discussion. It would allow to study both polarized e - p and polarized p - p (fixed target) interactions. Gluon polarization can be determined from charm and from di-jet production, as in the COMPASS experiment, but in a broader kinematic range. Such option is unlikely before the year 2005.

8. Conclusion

The COMPASS experiment will determine gluon polarization, $\Delta G/G$, from virtual photon-gluon fusion leading to open charm (D^0 and D^{*+}) and to correlated, high- p_t h^+h^- production. From charm production, after two years of data taking (150 days/year, 25% overall efficiency) with 100 GeV

muon beam and with NH_3 and ${}^6\text{LiD}$ targets (used in the proportion 1:1.5), the precision $\delta(\Delta G/G)$ will be ~ 0.1 . Using correlated, high- p_t hadron pairs, after one year of data taking with 200 GeV beam and the ${}^6\text{LiD}$ target, this precision will be ~ 0.05 . In the first measurement the error comes from the statistics while in the second one it is due to uncertainties in the PGF and Compton cross sections. In these two measurements the asymmetries from PGF are expected to have opposite sign.

The asymmetry in h^+h^- production has large contribution from the Compton process, which is however more important at higher x_g and has positive asymmetry. Positive gluon polarization gives rise to negative PGF asymmetry. Therefore the measured asymmetry in h^+h^- production is expected to change sign from small to large x_g .

The COMPASS experiment is expected to start data taking in the year 2000. Independent results might come from experiments at RHIC and from the HERMES at DESY.

I would like to thank organizers for interesting conference and for the invitation to present COMPASS experiment. I am grateful to A. Bravar for discussions and for providing me with plots presented in this paper.

REFERENCES

- [1] EMC; J. Ashman *et al.*, *Phys. Lett.* **B206**, 364 (1988); *Nucl. Phys.* **B328**, 1 (1989).
- [2] SMC; B. Adeva *et al.*, *Phys. Lett.* **B412**, 414 (1997).
- [3] SMC; D. Adams *et al.*, *Phys. Lett.* **B396**, 338 (1997).
- [4] E142; P.L. Anthony *et al.*, *Phys. Rev. Lett.* **71**, 959 (1993); *Phys. Rev.* **D54**, 6620 (1996).
- [5] E143; K. Abe *et al.*, *Phys. Rev. Lett.* **74**, 346 (1995).
- [6] E143; K. Abe *et al.*, *Phys. Rev. Lett.* **75**, 25 (1995).
- [7] E154; K. Abe *et al.*, *Phys. Rev. Lett.* **79**, 26 (1997).
- [8] E155; A. Brüll, The Spin Structure of the Nucleon, XVIII International Symposium on Lepton-Photon Interactions, 28 July–1 August 1997, Hamburg.
- [9] K. Ackerstaff *et al.*, OAP-741 and hep-ex/9703005.
- [10] J.D. Bjorken, *Phys. Rev.* **148**, 1167 (1996); **D1**, 1376 (1970).
- [11] S.A. Larin, *Phys. Lett.* **B334**, 192 (1994).
- [12] M. Glück, E. Reya, M. Stratmann, W. Vogelsang, *Phys. Rev.* **D53**, 4775 (1996).
- [13] R.D. Ball, S. Forte, G. Ridolfi, *Phys. Lett.*, **B378**, 255 (1996).
- [14] T. Gehrmann, W.J. Stirling, *Z. Phys.* **C65**, 461 (1995); *Phys. Rev.* **D53**, 6100 (1996).

- [15] G. Altarelli, R.D. Ball, S.Forte, G. Ridolfi, *Nucl. Phys.* **B496**, 337 (1997).
- [16] R.G. Roberts, The structure of the proton, Cambridge Monographs on Mathematical Physics (1990).
- [17] R. Devenish, Structure Functions, plenary session, International Europhysics Conference on High Energy Physics, 19–26 August 1997, Jerusalem.
- [18] A. Priniias, F_2^c , F_L and gluon determination at HERA, parallel session, International Europhysics Conference on High Energy Physics, 19–26 August 1997, Jerusalem.
- [19] E154; K. Abe *et al.*, SLAC-PUB-7460 (1997) and hep-ex/9705017.
- [20] COMPASS; “COMPASS Proposal”, CERN/SPSLC 96-14, SPSLC/P297 (1996) and CERN/SPSLC 96-30 (1996).
- [21] P. Nason, S. Dawson, R.K. Ellis, *Nucl. Phys.* **B303**, 607 (1988); R.K. Ellis, P. Nason, *Nucl. Phys.* **B312**, 551 (1989); W. Beenakker *et al.*, *Phys. Rev.* **D40**, 54 (1989); *Nucl. Phys.* **B351**, 507 (1991); J. Smith, W.L. van Neerven, *Nucl. Phys.* **B374**, 36 (1992); M. Mangano, P. Nason, G. Ridolfi, *Nucl. Phys.* **B373**, 295 (1992); E. Laenen, S. Riemersma, J. Smith, W.L. van Neerven, *Phys. Lett.* **B291**, 325 (1992); *Nucl. Phys.* **B392**, 162 (1993); S. Frixione, M. Mangano, P. Nason, G. Ridolfi, *Nucl. Phys.* **B412**, 225 (1994); B.W. Harris, J. Smith, *Nucl. Phys.* **B452**, 109 (1995); *Phys. Lett.* **B353**, 535 (1995).
- [22] M. Buza, Y. Matiounine, J. Smith, W.L. van Neerven, *Nucl. Phys.* **B485**, 420 (1997).
- [23] M. Glück, E. Reya, M. Stratmann, *Phys. Rev.* **D54**, 5515 (1996).
- [24] SMC; D. Adams *et al.*, *Phys. Rev.* **D56**, 5330 (1997).
- [25] ZEUS; M. Derrick *et al.*, *Phys. Lett.* **B349**, 225 (1995).
- [26] A.D. Watson, *Z. Phys.* **C12**, 123 (1982).
- [27] S. Frixione, M.L. Mangano, P. Nason, G. Ridolfi, *Nucl. Phys.* **B431**, 453 (1994).
- [28] T. Gehrmann, W.J. Stirling, *Z. Phys.* **C65**, 461 (1994).
- [29] NA14/2; M.P. Alvarez *et al.*, *Z. Phys.* **C60**, 53 (1993).
- [30] B. Andersson, G. Gustafson, G. Ingelman, T. Sjöstrand, *Phys. Rep.* **97**, 31 (1983); T. Sjöstrand, M. Bengtsson, *Comput. Phys. Commun.* **43**, 367 (1987).
- [31] G. Ingelman, J. Rathsman, G. Schuler, *Comput. Phys. Commun.* **101**, 135 (1997).
- [32] T. Sjöstrand, *Comput. Phys. Commun.* **82**, 74 (1994).
- [33] G. Ingelman, A. Edin, J. Rathsman, *Comput. Phys. Commun.* **101**, 108 (1997).
- [34] A. Bravar, D. von Harrach, A. Kotzinian, hep-ph/9710266 (1997).
- [35] A. Bravar, K. Kurek, R. Windmolders, *Comput. Phys. Commun.* **105**, 42 (1997).
- [36] M. Ruh, *Acta Phys. Pol.* **B29**, 1275 (1998), this issue and private communication.

- [37] M.E. Beddo *et al.*, Proposal on Spin Physics Using the RHIC Polarised Collider, April 1992 and Update, 1993.
- [38] A. De Roeck *et al.*, "Future Physics at HERA", in Proceedings of the Workshop 1995/96, ed. by G. Ingelman *et al.*, p.803; Y.I. Makdisi, Proc. 12th Int. Symposium on High Energy Spin Physics, Amsterdam 1996, ed. by C.W. de Jager *et al.*, World Scientific, Singapore 1997, p.107; V.W. Hughes, Proc. 12th Int. Symposium on High Energy Spin Physics, Amsterdam 1996, ed. by C.W. de Jager *et al.*, World Scientific, Singapore 1997, p.643; Proceedings of the workshop: Physics with Polarised Protons at HERA, ed. A. De Roeck, T. Gehrman, DESY-98-100.